[18F]F13640: a selective agonist PET radiopharmaceutical for imaging functional 5-HT1A receptors in humans

Pierre Courault (pierre.courault@chu-lyon.fr)
Hospices Civils de Lyon https://orcid.org/0000-0002-1654-4753
Sophie Lancelot
Universite Claude-Bernard: Universite Claude Bernard Lyon 1
Nicolas Costes
CNRS: Centre National de la Recherche Scientifique
Matthieu Colom
Hospices Civils de Lyon
Didier Le Bars
Hospices Civils de Lyon
Jérôme Redoute
Université Claude Bernard Lyon 1: Universite Claude Bernard Lyon 1
Florent Gobert
Hospices Civils de Lyon
Frédéric Dailler
Hospices Civils de Lyon
Sibel Isal
Hospices Civils de Lyon
Thibaut Iecker
CERMEP
Adrian Newman-Tancredi
Neurolixis
Inés Merida
Universite Claude-Bernard: Universite Claude Bernard Lyon 1
Luc Zimmer
Universite Claude-Bernard: Universite Claude Bernard Lyon 1 https://orcid.org/0000-0002-2805-7098

Research Article

Keywords: [18F]F13640, 5-HT1A receptors, functional receptor, PET imaging, brain, modelling study

Posted Date: May 26th, 2022

DOI: https://doi.org/10.21203/rs.3.rs-1675784/v1

Version of Record: A version of this preprint was published at European Journal of Nuclear Medicine and Molecular Imaging on January 19th, 2023. See the published version at https://doi.org/10.1007/s00259-022-06103-1.

Abstract

Purpose:

F13640 (a.k.a. befiradol, NLX-112) is a highly selective 5-HT_{1A} receptor ligand that was selected as a PET radiopharmaceutical-candidate based on animal studies. Due to its high efficacy agonist properties, [^{18}F]F13640 binds preferentially to functional 5-HT_{1A} receptors, which are coupled to intracellular G-proteins. Here we characterize brain labeling of 5-HT_{1A} receptors by [^{18}F]F13640 in humans and describe a simplified model for its quantification.

Methods:

PET/CT and PET-MRI scans were conducted in a total of 13 healthy male volunteers (29 ± 9 years old), with arterial input functions (AIF) and test-retest protocol. Several kinetic models were compared (one tissue compartment model, two-tissue compartment model and Logan); two models with reference region were also evaluated: simplified reference tissue model (SRTM) and the Logan reference model (LREF).

Results:

[^{18}F]F13640 showed high uptake values in raphe nuclei and cortical regions. SRTM and LREF models showed excellent correlation with kinetic models using AIF. Considering test-retest parameters and the prolonged binding kinetics of [^{18}F]F13640, better reproducibility and reliability were found with the LREF method. Cerebellum white matter and frontal lobe white matter stand out as suitable reference regions.

Conclusion:

The favorable brain labeling and kinetic profile of [^{18}F]F13640, its high receptor specificity and its high efficacy agonist properties open new perspectives for studying functionally active 5-HT_{1A} receptors, unlike previous radiopharmaceuticals that act as antagonists. [^{18}F]F13640's kinetic properties allow injection out of the PET scanner with delayed acquisitions, facilitating the design of innovative longitudinal protocols in neurology and psychiatry.

Trial Registration EudraCT 2017-002722-21

Introduction

Serotonin (5-hydroxytryptamine, 5-HT) is known to have a variety of functions in the central nervous system, which are mediated by a diversity of receptors. Among them, the serotonin 1A receptor subtype (5-HT_{1A}) is a G-coupled protein receptor (GCPR) which has attracted extensive interest because it is involved in regulation of mood, cognition, pain and movement [1]. Consequently, various positron emission tomography (PET) radiotracers have been developed to target 5-HT_{1A} receptors, including [O-*methyl*-^{11}C]WAY100635 [2], [*carbonyl*-^{11}C]WAY100635 [2, 3] and [^{18}F]MPPF, a fluorinated derivate of WAY100635 [4, 5]. [^{18}F]MPPF binding is observed mainly in brain regions with high density of 5-HT_{1A} receptors such as hippocampus and raphe nuclei [5–7] and it has been used to explore various psychiatric and neurologic diseases such as epilepsy [8],

narcolepsy [9], Alzheimer's disease [10] or multiple system atrophy [11]. Other derivatives of WAY100635 have been also proposed as radiopharmaceuticals but have been less used in human [12].

Nevertheless, although [^{11}C]WAY100635 and [^{18}F]MPPF are widely used for the *in vivo* exploration of 5-HT$_{1A}$ receptors, PET imaging using these radiopharmaceuticals remains limited in terms of pathophysiological interpretation because of their antagonist pharmacological properties. Indeed, antagonists bind both G protein-coupled and G-protein uncoupled receptors with the same affinity, labelling the total receptor population, regardless of its functional status. In contrast, agonists have higher affinity for their target GPCRs when the latter are coupled to G-proteins, *i.e.*, they are in a functional state which is directly associated with neurotransmission [13, 14]. Thus, we hypothesized that highly specific 5-HT$_{1A}$ receptor agonist radiotracers would constitute useful tools to explore endogenous serotonergic neurotransmission and pathophysiological changes that specifically affect functional receptors and which would not be detectable using antagonist radiopharmaceuticals [15].

Very few 5-HT$_{1A}$ agonists have been used as chemical templates to develop a PET radiopharmaceutical. [^{11}C]CUMI-101, which was initially presented as an agonist, was later found to act as a partial agonist or even as an antagonist [16], and it also binds to α_1 adrenoceptors [17]. These suboptimal pharmacological properties explain its modest sensitivity to pharmacological challenges or to endogenous serotoninergic changes in human [18, 19]. In this context, we chose to use highly specific and pharmacologically well characterized 5-HT$_{1A}$ receptor agonists to develop the corresponding radiopharmaceuticals. Following several studies, we selected F13640 (a.k.a. befiradol or NLX-112), which possesses high affinity (nanomolar Ki) for 5-HT$_{1A}$ receptors, high selectivity (> 1000-fold) over a large range of other CNS targets and whose chemical structure includes a fluorine which is substitutable by a fluorine-18. As a result, [^{18}F]F13640 was proposed as the first preclinical fluorinated 5-HT$_{1A}$ receptor agonist radiopharmaceutical, supported by compelling preclinical data in animal models [20, 21]. Although a first image obtained in a healthy volunteer suggested favorable brain penetration by [^{18}F]F13640 [22], it remained to be demonstrated whether [^{18}F]F13640 could become a usable radiopharmaceutical for future clinical investigation. The objectives of the present study were, therefore, to perform a full PET kinetic modelling of [^{18}F]F13640 using arterial input function (AIF), to identify a reference region suitable for a simplified modelling method, and to assess reproducibility with test-retest scans. Ultimately, the present data characterizing [^{18}F]F13640 as a selective agonist radiopharmaceutical will, for the first time, enable investigation of changes in 5-HT$_{1A}$ receptor expression and functionality in patients suffering from disorders arising from dysfunctional serotonergic neurotransmission.

Material And Methods

Synthesis and quality control

[^{18}F]F13640 (3-chloro-4-fluorophenyl)-[4-^{18}fluoro-4-[[(5-methylpyridin-2-yl)methylamino]methyl]piperidin-1-yl]methanone; a.k.a. [^{18}F]NLX-112 or [^{18}F]befiradol) was synthesized as previously described [21]. Briefly, radiolabelling was obtained by a nucleophilic fluoro-substitution on the F13640 nitro precursor using an

automated radiosynthesizer (Neptis, ORA). Chemical and radiochemical purity measured by HPLC were higher than 95%. Mean molar activity (EOS) was 87 ± 18 GBq/µmol.

Study design

The study was performed according to the ethical standards of the institutional and national research committee and with the principles of the 1964 Declaration of Helsinki. The study was approved by a French ethics committee (Eudra-CT: 2017-002722-21) and pre-registered on the ClinicalTrials.gov database (NCT03347331).

Participants were healthy volunteers, *i.e.*, without neurological or psychiatric disorders, active infectious disease, severe and progressive medical pathology, without addiction (smoking, cannabis, alcohol…) or MRI and PET contraindications. Twenty volunteers were screened in the study and signed consent. Two volunteers failed inclusion due to exclusion criteria (MRI contraindication and body weight superior to 90 kg). The first eight volunteers were included in a pilot study. In this pilot study, subjects performed an anatomical MRI scan (3D T1-weighted sequence on a 1.5-T Siemens Magneton scanner, Siemens AG, Erlanger, Germany) and a 90 min PET/CT (Siemens Biograph mCT64) scan with arterial input function (AIF, data not shown). The later 10 volunteers were included to perform a test-retest protocol with two PET-MRI scans as described below. Four participants had AIF measurements on one of the two visits. Two volunteers were lost to follow-up. To sum up, data analysis focused on four participants when concerning PET modelling with AIF and eight participants for test-retest analysis. Figure 1 summarizes recruitment of healthy subjects in the study.

PET-MRI test-retest protocol

Participants underwent a PET-MRI acquisition on the Siemens mMR Biograph system. Because the pilot study group scans showed that [^{18}F]F13640 had very slow kinetics, an acquisition of almost four hours was necessary. Thus, for the comfort of the subjects, the acquisition was carried out in two parts. In part 1, list-mode PET data were acquired for 90 min directly after the injection of [^{18}F]F13640 (150 MBq + 1MBq/kg ± 10%) (PET1, [0; 90] min. post injection). Subjects were then taken out of the camera for a break. One hour later, for part 2, subjects had a second PET-MRI scan for 75 min (PET2; [150; 225] min. post injection). Participants performed this PET-MRI protocol twice (test and retest sessions) one to nine weeks apart.

During PET1, a 3D T1 MPRAGE MRI was acquired in sagittal orientation, with a matrix size of 256 × 256 × 176 and a voxel size of 1 mm iso. TR/TE was 3300/2.45 ms, TI 1100ms, and flip angle 8°. A quicker T1 MPRAGE MRI was acquired at the beginning of PET2 to accurately register data from the two sessions (sagittal acquisition, matrix size 256 × 256 × 176, voxel size 1 mm iso, TR/TE 1800/2.34 ms, TI = 850 ms, flip angle 8).

PET-MRI image processing

The PET data from the two parts were reconstructed independently. First, a MR-based attenuation correction map was generated from the T1 MPRAGE of each part [23]. PET1 and PET2 list-modes were then corrected for motion with EBER algorithm [24]. PET1 was rebinned into 24 frames of variable duration (8 × 15 s, 3 × 60 s, 5 × 120 s, 1 × 300 s, 7 × 600 s) and PET2 was rebinned into 8 frames (7 × 600 s, 1 × 300 s). Sinograms

were corrected for attenuation, scatters, randoms and normalization. PET reconstructions were performed with Siemens e7tools using the OP-OSEM algorithm with PSF, 3 iterations and 21 subsets. A matrix size of 256 and a zoom of 3 were applied yielding a voxel size of 0.93 × 0.93 × 2.03 mm with a 4 mm 3D post-reconstruction gaussian filtering.

Both dynamic PET series from PET1 and PET2 were combined in a single dynamic series in the following way. The mean of each dynamic PET series was computed. The mean of PET2 was rigidly coregistered to the mean of PET1. This rigid transformation was applied to all frames of PET2 to obtain the PET2 frames aligned with the PET1 frames. Decay correction was applied to PET2 and PET1 setting the reference time for both series to the start time of PET1 scan. PET1 and PET2 were finally concatenated in a single and harmonized dynamic 4D file. These preprocessing steps were performed with the minc toolkit functions (http://bic-mni.github.io).

Besides, test and retest PET-MRI sessions were coregistered through the co-registration of the T1 image of retest session to the T1 image of the test session, applying the computed rigid coregistration matrix to all images of the retest session. The structural T1 image from test session was automatically segmented into anatomical regions using the multi-atlas propagation with enhanced registration (MAPER) method [25], and the 95-region Hammersmith atlas [26–28]. The regional segmentation was projected to test and retest sessions, and regional time activity curves (TAC) were extracted for a selection of brain regions. Regions selected for analysis were cortical regions (cingulate, frontal, occipital, parietal, temporal superior and temporal inferior), amygdala, central grey nuclei, hippocampus, insula, parahippocampal gyrus, thalamus, brainstem, dorsal and median raphe nuclei, cerebellum (total, grey matter, and white matter), vermis, frontal lobe white matter and corpus callosum.

Arterial input function (AIF)

Four participants underwent AIF measures during their test or retest session. AIF, free fraction, and metabolites were measured based on 29 blood samples. Samples were collected manually after arterial catheterization with local anaesthesia (lidocaine patch 5%). Sample time points were as follows: every 5 seconds in the first minute, every 15 seconds until second minute, every 30 seconds until third minute and at time 5, 10, 20, 30, 40, 60, 75, 90, 160 and 205 minutes. Whole blood radioactivity was counted on every sample using a gamma counter (Perkin-Elmer) to measure the whole blood curve (Cwb). Plasma was collected and counted after centrifugation (4 min, 3000 G at 4°C) on 18 out of 29 samples (t = 15 s and every sample after the first minute to calculate plasma to whole blood ratio f_{wb}). Uncorrected plasma curve (*Cp*) was determined by the mean f_{wb} and the whole blood curve: $Cp(t) = f_{wb}.Cwb(t)$. On 5 samples (t = 2, 10, 30, 90 and 205 min) free fraction and metabolites were determined. For metabolites, 500 µL of plasma were added to 750 µL of acetonitrile with cold carrier of F13640 at 20 mg/L, centrifuged (4 min, 3000 G at 4°C), filtered at 0.45 µm, diluted with water and injected in a C8 HPLC column with a mixed mobile phase water/acetonitrile/TFA (60/40/0.1). Metabolites and [^{18}F]F13640 were separated and fractions were collected and counted in the gamma counter. The activity of the [^{18}F]F13640 fraction was divided by the total activity recovered from the gamma counter to give plasma parent fraction of unmetabolized [^{18}F]F13640 (PPf). For plasma free fraction (*fp*), 1 mL of plasma was centrifugated (Centrifree®, Millipore) for 20 min, 2000g at 20–25°C and 100 µL of ultrafiltrate plasma was counted in gamma counter. After counting, all samples were

weighed, and counts corrected. The *fp* was calculated from the ratio of concentrations in the ultrafiltrate and whole plasma. AIF was the plasma curve corrected from the plasma parent fraction curve and free fraction: *AIF(t) = PPf(t).Cp(t).fp(t).*

Kinetic modelling

Cerebral TACs were modeled with three different AIF models for participants who performed AIF (n = 4): one tissue compartment (1TC), two-tissue compartment (2TC) and the Logan graphical method (LOGAN) [29]. Model fit accuracy were compared using the Akaike Information Criterion (AIC). Two models with reference region were also assessed: the Simplified Reference Tissue Model (SRTM) [30] and the logan reference model (LREF) [29]. The use of four different reference regions were compared: corpus callosum (CC), cerebellum (CER), white matter cerebellum (CERWM) and frontal lobe white matter (FLWM). Distribution volume ratio (DVR) for models with AIF (DVR_{1TC} or DVR_{2TC}) were calculated as the ratio between Vt of the region of interest and the Vt of the reference region. DVRs for SRTM (DVR_{SRTM}) were calculated by adding one to the binding potential (BP) value. DVRs calculated with AIF models were compared to DVRs obtained with reference region models using linear regression to determine fitting parameters: intercept, slope and determination coefficient (R^2). Kinetic modelling was done using the Turku PET center utilities library (TPCCLIB, https://gitlab.utu.fi/vesoik/tpcclib).

Test-retest reproducibility and reliability

For all the participants in the test-retest study (n = 8), models with reference region were performed on both sessions. Bias and variability (VAR) were calculated to assess reproducibility and the intraclass correlation coefficient (ICC) for reliability. Bias was calculated as (DVR_{retest} – DVR_{test}) / DVR_{test} x 100 and VAR as the standard deviation (SD) of the bias. Parameters were expressed as percentage. ICC was calculated as (BSMSS-WSMSS)/(BSMSS + WSMSS) where the BSMSS is the mean sum of square between subjects and WSMSS is the mean sum of square within subjects [31].

Statistical analysis

Statistical analysis was performed using RStudio (RStudio Team 2020, http://www.rstudio.com/). Paired Student's t-tests were used to assess differences between injected doses and molar activities between test and retest sessions. Significant threshold was set at $p < 0.05$.

Results

Subject demographics

Mean age of the participants was 29 ± 9 years in the test-retest study. No significant differences were found in the activity of the [^{18}F]F13640 doses administered to the subjects or in the molar activities of [^{18}F]F13640 between test and retest (p-value < 0.05). Due to an injection error, participant 8 received a dose of [^{18}F]F13640 for retest session that was slightly lower than the recommended dosages described in the study. Details are presented in Table 1.

Table 1
Age, activity injected dose and molar activity per subject and test and retest session. No significant differences were found between test and retest sessions (p-value > 0.05).

		Test Session		Retest Session	
Subject	Age	Activity injected (MBq)	Molar activity (GBq/μmol)	Activity injected (MBq)	Molar activity (GBq/μmol)
1	25	211	75	214	79
2	28	213	71	219	83
3	23	213	75	224	108
4	23	210	78	227	76
5	45	232	72	257	126
6	21	210	87	222	81
7	42	226	75	243	105
8	27	243	124	188	76
Mean ± SD	29 ± 9	220 ± 12	82 ± 18	224 ± 20	92 ± 19

Modelling study

Mean plasma parent fractions were 99.40 ± 0.00%, 97.40 ± 0.01%, 96.20 ± 0.01%, 95.40 ± 0.01% and 95.30 ± 0.01% at 2, 10, 30, 90 and 205 minutes respectively after injection. One value was discarded for participant 2 at 90 minutes due to non-interpretable value. Mean plasma parent fraction was modelled with a one-exponential function:

$$\mathrm{PP}f(t) = 1 - A_0.(1 - e^{\left(-\ln(2)*\frac{t}{T}\right)})$$

with A_0 = 0.046 and T = 9.06 min

Free plasmatic fraction was not constant over time and mean values were 0.48 ± 0.09%, 0.82 ± 0.08%, 1.14 ± 0.26%, 1.90 ± 0.71% and 1.61 ± 0.29% at 2, 10, 30, 90 and 205 minutes. Ratio plasma to whole blood was stable over time and mean value was 1.79 ± 0.03. Table 2 resumes pharmacokinetic parameters for each subject. Figure 2 shows an example of AIF corrected for metabolites and free fraction, whole blood, and uncorrected plasma curves.

Table 2
Details of pharmacokinetics parameters per subject. Plasma parent fraction and free plasma fraction results are expressed as function of time. Plasma to whole blood was stable over time and results are expressed as mean value across the sessions for each participant.

Parameter	**Plasma Parent Fraction (%)**					**Free Plasma Fraction (%)**					**Plasma to Whole Blood Ratio**
Time (min) Subject	2	10	30	90	205	2	10	30	90	205	Mean value ± SD
2	99.5	96.1	95.4	NA	96.7	0.42	0.72	1.10	1.23	1.94	1.84 ± 0.11
5	99.5	97.9	97.8	96.7	95.6	0.52	0.79	0.88	2.87	1.66	1.78 ± 0.11
7	98.9	97.5	95.8	94.9	94.7	0.38	0.88	1.08	1.56	1.62	1.77 ± 0.14
8	99.5	98.0	95.6	94.5	94.3	0.59	0.89	1.51	1.94	1.24	1.77 ± 0.14
Mean ± SD	*99.40 ± 0.00*	*97.40 ± 0.01*	*96.20 ± 0.01*	*95.40 ± 0.01*	*95.30 ± 0.01*	*0.48 ± 0.09*	*0.82 ± 0.08*	*1.14 ± 0.26*	*1.90 ± 0.71*	*1.61 ± 0.29*	*1.79 ± 0.03*

Mean AIC using one-tissue compartment model (1TC) was 320.88 ± 13.66 and 291.92 ± 25.46 for the two-tissue compartment model (2TC). Two-tissue compartment model better fits with the pharmacokinetic of [^{18}F]F13640 when comparing the AIC. However, the 1TC model was considered as the reference model for results presented below due to non-interpretable kinetics parameter (k_3 and k_4) when 2TC model was used.

Pharmacokinetic parameters for the 1TC model are presented in Table 3. The highest Vt values were found in raphe nuclei (median and dorsal), cingulate, amygdala and insula. The lowest Vt values were in cerebellum white matter, frontal lobe white matter and corpus callosum, all tested as reference regions. Cerebellum (grey + white matter), also tested as a reference region, showed intermediate Vt values.

Table 3
Mean binding potential value for kinetic one-tissue compartment model parameters for 4 subjects. Data are presented as mean ± SD.

Regions	K1 (mL/(min*mL))	k2 (min^{-1})	Vt (mL/mL)	Vb (%)
Cortical Region				
Cingulate Lobe	1.38 ± 0.31	0.014 ± 0.004	98.4 ± 19.6	3.8 ± 0.4
Frontal Lobe	1.33 ± 0.24	0.016 ± 0.004	86.9 ± 19.4	3.3 ± 0.3
Occipital Lobe	1.26 ± 0.28	0.017 ± 0.004	77.9 ± 17.5	3.6 ± 0.4
Parietal Lobe	1.32 ± 0.33	0.016 ± 0.004	83.6 ± 19.4	3.8 ± 0.3
Temporal Superior Lobe	1.31 ± 0.29	0.016 ± 0.004	85.5 ± 20.7	4.0 ± 0.8
Temporal Inferior Lobe	1.19 ± 0.29	0.016 ± 0.004	78.2 ± 20.0	2.9 ± 0.4
Subcortical Region				
Amygdala	1.07 ± 0.22	0.013 ± 0.003	87.8 ± 20.2	3.6 ± 0.6
Central Grey Nuclei	1.07 ± 0.27	0.016 ± 0.004	71.3 ± 18.5	3.0 ± 0.5
Hippocampus	1.04 ± 0.25	0.013 ± 0.003	83.3 ± 19.8	3.5 ± 0.6
Insula	1.18 ± 0.26	0.014 ± 0.004	88.1 ± 21.3	3.7 ± 0.4
Parahippocampal gyrus	1.05 ± 0.21	0.014 ± 0.004	75.8 ± 15.9	4.4 ± 0.8
Thalamus	1.18 ± 0.28	0.015 ± 0.004	84.4 ± 21.6	3.8 ± 0.3
Brainstem				
Brainstem	1.03 ± 0.26	0.013 ± 0.003	81.6 ± 21.6	3.3 ± 0.4
Dorsal Raphe Nucleus	1.21 ± 0.33	0.013 ± 0.004	96.6 ± 28.4	3.3 ± 0.5
Median Raphe Nucleus	1.13 ± 0.31	0.012 ± 0.003	93.8 ± 26.0	3.2 ± 0.5
Cerebellum				
Cerebellum	1.38 ± 0.37	0.016 ± 0.004	86.6 ± 20.4	4.2 ± 0.4
Cerebellum Grey Matter	1.38 ± 0.41	0.016 ± 0.004	86.6 ± 22.0	4.1 ± 0.4
Cerebellum White Matter	1.03 ± 0.25	0.015 ± 0.003	68.7 ± 16.9	2.8 ± 0.3
Vermis	1.41 ± 0.40	0.017 ± 0.004	86.7 ± 22.0	3.9 ± 0.4
Reference region				
Frontal Lobe White Matter	0.81 ± 0.16	0.013 ± 0.004	63.3 ± 13.7	2.0 ± 0.3
Corpus Callosum	0.56 ± 0.11	0.011 ± 0.003	49.8 ± 9.9	2.2 ± 0.4

Linear regressions of DVR_{LREF} and DVR_{SRTM}, compared to DVR_{1TC} with the four reference regions tested, are presented in Table 4. For LREF model, all coefficients of determination (R^2) were excellent (> 0.9). Best fitting was obtained with $LREF_{CERWM}$ and $LREF_{CER}$ (0.95 ± 0.03 both). Noted that $LREF_{CC}$ and $LREF_{FLWM}$ showed excellent R^2 (0.94 ± 0.03 and 0.94 ± 0.04 respectively). Intercept ranged from 0.01 ± 0.05 ($LREF_{CER}$) to 0.04 ± 0.08 ($LREF_{CC}$) thus best fitting (closest to 0) was obtained with $LREF_{CER}$. Slopes were excellent, from 0.93 ± 0.02 ($LREF_{CC}$) to 1.01 ± 0.03 ($LREF_{CERWM}$) and best slope (closest to 1) was found with $LREF_{CERWM}$ (1.01 ± 0.02). For SRTM model, regression parameters (R^2) were slightly lower than those found with LREF but close to 0.9, except for CC which showed the worse R^2 (0.59 ± 0.10). Intercepts ranged from 0.04 ± 0.09 for $SRTM_{CER}$ (best fitting) to 0.68 ± 0.12 for $SRTM_{CC}$. Slopes were satisfying, ranging from 0.67 ± 0.13 ($SRTM_{CC}$) to 0.93 ± 0.13 ($SRTM_{CER}$). $SRTM_{CERWM}$ and $SRTM_{FLWM}$ showed acceptable slopes with 0.92 ± 0.09 and 0.91 ± 0.10 respectively.

Table 4
Regression parameter of DVR_{SRTM} and DVR_{LREF} compared to DVR_{1TC} for 4 subjects with AIF. Test-retest parameters for reproducibility assessment in 8 healthy subjects. Reference region tested were corpus callosum (CC), cerebellum (CER), cerebellum white matter (CERWM) and frontal lobe white matter (FLWM). Data are presented as mean ± SD. ICC = interclass correlation coefficient, VAR = variability.

	Mean regression parameter compared to DVR_{1TC}				**Mean test-retest parameters**		
Model	Reference Region	Slope	Intercept	R^2	ICC	Bias (%)	VAR (%)
DVR_{LREF}	CC	0.93 ± 0.02	0.04 ± 0.08	0.94 ± 0.03	0.89 ± 0.10	0.95	2.84
	CER	1.01 ± 0.03	0.01 ± 0.05	0.95 ± 0.03	0.93 ± 0.13	-0.27	2.81
	CERWM	1.01 ± 0.02	0.02 ± 0.06	0.95 ± 0.03	0.95 ± 0.04	-0.04	2.41
	FLWM	0.97 ± 0.03	0.03 ± 0.08	0.94 ± 0.04	0.88 ± 0.08	0.24	2.55
DVR_{SRTM}	CC	0.67 ± 0.13	0.68 ± 0.12	0.59 ± 0.10	0.67 ± 0.17	0.23	11.34
	CER	0.93 ± 0.13	0.04 ± 0.09	0.90 ± 0.03	0.75 ± 0.26	-0.55	7.16
	CERWM	0.92 ± 0.09	0.10 ± 0.06	0.89 ± 0.03	0.63 ± 0.23	-1.48	8.76
	FLWM	0.91 ± 0.10	0.14 ± 0.09	0.90 ± 0.10	0.47 ± 0.31	0.34	8.51

Parametric images were obtained using models with reference region. As an example, Fig. 3 shows brain parametric image of binding potential (BP) using LREF modelling method with CERWM as reference region.

Test-retest reproducibility and reliability

Test-retest study results are presented in Table 4. Reproducibility showed excellent results for LREF method and satisfying results for SRTM. Biases were almost similar between modelling methods and between reference regions. Results ranged from − 1.48 to 0.95% with the lowest bias for $LREF_{CERWM}$ (-0.04%). Considering variability (VAR), results were more disparate between methods. LREF method showed excellent variability less than 3% for all reference regions. Lowest VAR was found for $LREF_{CEWRM}$ with 2.41%. VARs for other reference regions were also excellent with 2.55%, 2.81% and 2.84% for $LREF_{FLWM}$, $LREF_{CER}$, $LREF_{CC}$ respectively. SRTM showed higher values. Lowest VAR was $SRTM_{CER}$ with 7.16%. Variability for $SRTM_{CERWM}$ and $SRTM_{FLWM}$ were also satisfying with 8.76% and 8.51% respectively. Reliability showed better results for LREF method than with SRTM, with all ICC around 0.9 and best performance for $LREF_{CERWM}$ (0.95 ± 0.04). STRM method showed ICCs were quite lower, with a wider extent ranging from 0.47 ± 0.31 for $SRTM_{FLWM}$ to 0.75 ± 0.26 for $SRTM_{CER}$. ICCs for $SRTM_{CERWM}$ and $SRTM_{CC}$ were intermediate with 0.63 ± 0.23 and 0.67 ± 0.17 respectively.

Table 5 summarizes reproducibility and reliability parameters in each region for $SRTM_{CERWM}$ and $LREF_{CERWM}$. DVR were highly correlated between test and retest whatever the method used ($R^2 > 0.99$ for $LREF_{CERWM}$ and $R^2 > 0.98$ for $SRTM_{CERWM}$). ICC, bias, and VAR per region confirmed results described in Table 4 and showed overall best parameters with $LREF_{CERWM}$ method.

Table 5

Reliability and reproducibility parameters between test and retest per region for Logan graphical method (LREF) and Simplified Reference Tissue Model (SRTM) using white matter cerebellum as reference region (CERWM). Parameters calculated were interclass correlation coefficient (ICC), variability (VAR) and bias. DVRs are expressed as mean ± SD. (CERGM = cerebellum grey matter; FLWM = frontal lobe white matter).

Model	Region	DVR test	DVR retest	ICC	Bias (%)	VAR (%)
$LREF_{CERWM}$	*Cortical Region*					
	Cingulate	1.38 ± 0.11	1.37 ± 0,10	0.97	0.31	1.78
	Frontal	1.28 ± 0.09	1.28 ± 0,09	0.97	0.54	1.80
	Occipital	1.06 ± 0.10	1.06 ± 0,09	0.99	-0.24	1.64
	Parietal	1.20 ± 0.10	1.20 ± 0,09	0.97	-0.30	2.16
	Temporal Inferior	1.15 ± 0.10	1.15 ± 0,09	0.92	-0.01	3.42
	Temporal Superior	1.24 ± 0.09	1.24 ± 0,09	0.93	-0.19	2.95
	Subcortical Region					
	Amygdala	1.20 ± 0.07	1.19 ± 0,06	0.90	0.07	2.28
	Central Grey Nuclei	1.03 ± 0.16	1.03 ± 0,15	0.94	0.38	2.30
	Hippocampus	1.15 ± 0.07	1.15 ± 0,06	0.92	-0.37	2.10
	Insula	1.22 ± 0.08	1.21 ± 0,08	0.94	0.55	2.42
	Parahippocampal gyrus	1.08 ± 0.08	1.09 ± 0,07	0.95	-0.79	2.47
	Thalamus	1.16 ± 0.09	1.15 ± 0,08	0.99	0.48	1.20
	Brainstem					
	Brainstem	1.12 ± 0.09	1.12 ± 0.08	0.99	0.25	1.09
	Dorsal Raphe Nucleus	1.33 ± 0.12	1.33 ± 0.11	0.94	0.25	3.12
	Median Raphe Nucleus	1.26 ± 0.12	1.27 ± 0.14	0.81	-1.27	6.62
	Cerebellum					
	Cerebellum	1.31 ± 0.07	1.31 ± 0.07	0.96	0.23	1.50
	CERGM	1.31 ± 0.07	1.31 ± 0.07	0.96	0.23	1.50
	Vermis	1.32 ± 0.07	1.32 ± 0.07	0.98	0.20	0.92
	Reference Region					
	FLWM	0.89 ± 0.06	0.89 ± 0.05	0.97	-0.31	1.66
	Corpus Callosum	0.68 ± 0.06	0.68 ± 0.04	0.92	-0.93	2.84
$SRTM_{CERWM}$	*Cortical Region*					

Model	Region	DVR test	DVR retest	ICC	Bias (%)	VAR (%)
	Cingulate	1.36 ± 0.15	1.40 ± 0.14	0.74	-3.04	7.09
	Frontal	1.18 ± 0.16	1.23 ± 0.15	0.86	-4.33	6.26
	Occipital	0.97 ± 0.13	0.99 ± 0.13	0.69	-1.49	11.95
	Parietal	1.11 ± 0.14	1.13 ± 0.12	0.70	-2.36	10.28
	Temporal Inferior	1.09 ± 0.17	1.11 ± 0.10	0.62	-2.72	11.15
	Temporal Superior	1.18 ± 0.19	1.21 ± 0.13	0.48	-3.04	14.74
	Subcortical Region					
	Amygdala	1.30 ± 0.14	1.30 ± 0.12	0.65	0.08	7.90
	Central Grey Nuclei	0.99 ± 0.18	1.01 ± 0.17	0.77	-1.96	6.84
	Hippocampus	1.24 ± 0.11	1.20 ± 0.12	0.62	3.11	7.34
	Insula	1.24 ± 0.15	1.26 ± 0.14	0.73	-1.58	8.55
	Parahippocampal gyrus	1.08 ± 0.08	1.08 ± 0.07	0.95	0.18	2.49
	Thalamus	1.15 ± 0.15	1.16 ± 0.12	0.79	-1.50	7.75
	Brainstem					
	Brainstem	1.21 ± 0.13	1.21 ± 0.15	0.88	0.30	6.54
	Dorsal Raphe Nucleus	1.41 ± 0.11	1.42 ± 0.17	0.55	-0.69	9.70
	Median Raphe Nucleus	1.36 ± 0.21	1.39 ± 0.18	-0.07	-2.23	20.03
	Cerebellum					
	Cerebellum	1.25 ± 0.07	1.26 ± 0.06	0.33	-0.93	5.60
	CERGM	1.25 ± 0.06	1.27 ± 0.05	0.35	-1.83	5.17
	Vermis	1.23 ± 0.07	1.24 ± 0.08	0.74	-1.12	4.46
	Reference Region					
	Corpus Callosum	0.77 ± 0.11	0.80 ± 0.08	0.63	-2.97	10.65
	FLWM	0.90 ± 0.07	0.92 ± 0.10	0.58	-2.92	7.61

Considering $LREF_{CERWM}$, bias was excellent, between − 1% and 1%, for all regions. Only median raphe nucleus showed bias outside this range (-1.27%). Variability was excellent for all regions around or less than 3%, except for median raphe nucleus (6.62%). Reliability was excellent (> 0.7) for all regions. Considering $SRTM_{CERWM}$, biases were all satisfying, higher value for frontal cortex (-4.33%) and hippocampus (3.11%). For variability, median raphe nucleus showed the highest value (20.03%). Temporal (superior and inferior), occipital, parietal cortex, and corpus callosum showed VAR higher than 10%. Other regions showed variability,

less than 10%. Reliability was low for median raphe nucleus (-0.07), cerebellum (0.33) and cerebellum grey matter (CERGM = 0.35). Some regions showed excellent reliability with ICCs superior to 0.7 such as cingulate (0.74) and frontal cortex (0.86), and best was found for parahippocampal gyrus (0.95). Other regions showed intermediate ICC from 0.5 to 0.7 such as hippocampus (0.62) and amygdala (0.65).

Discussion

In this study we describe the first-in-human trial of a new PET radiopharmaceutical [^{18}F]F13640 which, thanks to its agonist properties, permits *in vivo* imaging of functional human 5-HT$_{1A}$ receptors. Several analyses were carried out: (i) full kinetic modelling of the radiopharmaceutical using dynamic scans and an AIF collection; (ii) comparison of four different reference regions and evaluation of two simplified modelling methods to measure binding potential values and obtain parametric images; and (iii) assessment of test-retest reliability for simplified models. The main finding is that [^{18}F]F13640 constitutes a 5-HT$_{1A}$ receptor radiopharmaceutical with favorable brain binding properties and the present study describes a PET acquisition protocol and a quantification method suitable for the clinical study of functional 5-HT$_{1A}$ receptors in neurology and psychiatry.

Study design

Initial tests used a protocol with 90 min PET/CT scans and AIF for study participants. However, preliminary analyses of the 5 first subjects revealed a slow intracerebral kinetic of the radiopharmaceutical implying that they did not reach a steady-state at 90 min after injection (online resource 1), a characteristic that has also been observed for some other radiopharmaceuticals, such as [^{18}F]fallypride [32]. The slow labeling kinetic of [^{18}F]F13640 and its high affinity for the target sites led to a long-term binding on 5-HT$_{1A}$ receptors in the present human study, an observation which is in accordance with our preclinical observations in rat, cat and macaque [21]. On the bases of these preliminary observations, we concluded that kinetic modelling of the tracer and parameters identification would require a longer acquisition protocol, which was then implemented for the main study. A 165-min long PET acquisition was implemented with a first scan lasting 90 min and a second one lasting 75 min, separated by a one-hour break outside of the camera. This longer protocol with two acquisition periods was facilitated using a hybrid PET-MR scanner, which is capable of brain anatomical realignment and motion correction between PET acquisitions.

Modelling study

Our data revealed that the pharmacokinetic parameters of [^{18}F]F13640 were similar to those found with F13640 (i.e., NLX-112, befiradol) at pharmacological doses. Thus, the fraction of [^{18}F]F13640 parent compound remained high (95%) in blood at 30 to 205 min after injection, consistent with observations on unlabeled NLX-112 in healthy volunteers (Neurolixis, data on file). Also, the free blood fraction of about 2% was similar between NLX-112 and [^{18}F]F13640. Finally, the ratio of [^{18}F]F13640 binding in plasma to whole blood showed favorable results with a preferentially distribution in plasma (1.79 ± 0.03). Altogether, these distribution characteristics of [^{18}F]F13640 were consistent with a facilitated brain distribution.

A crucial step in the validation of a new brain receptor radiopharmaceutical is the validation of a reference region. Based on literature describing regions poor in 5-HT_{1A} receptors, we tested four different reference regions: corpus callosum (CC), cerebellum (CER), cerebellum white matter (CERWM) and frontal lobe white matter (FLWM). We tested their accuracy and reproducibility performance with two simplified modelling methods, the Logan Reference Model (LREF) and the Simplified Reference Tissue Method (SRTM). For the validation with a gold standard, excellent correlations have been found with the LREF model compared to the 1TC AIF, whatever the reference region. The SRTM method also showed satisfying results in regression with the 1TC AIF model, except for CC as reference, which showed the weakest results. For test-retest reproducibility, ICC, bias, and variability were similar for LREF with the four reference regions, with superior performance when using CERWM as reference region. With SRTM methods, performances for reliability are more mixed, with a clear superiority for the CERWM reference region. Combining these results, CERWM is the best reference region showing a low binding, an excellent correlation with AIF model and an excellent test-retest reproducibility. Both the LREF and SRTM methods showed close binding values for all brain regions. Using the SRTM method, amygdala and hippocampus showed high BP while LREF-calculated BP values were intermediate. According to 1TC model, the binding values of amygdala and hippocampus calculated with LREF are more accurate than the one with SRTM. However, considering test-retest parameters, better reproducibility and reliability were found with the LREF method. Excellent performance of test-retest variability is confirmed at the regional level for LREF with the CERWM, which is not systematically the case for SRTM and CERWM.

Overall, these results lead us to favor the LREF model with CERWM as reference region for future studies comparing patients to healthy volunteers or patients at different times. The low variability and excellent reliability (ICC > 0.7) of the LREF model with CERWM as reference region guarantee power of future studies and capacity to detect differences between groups due to pathological changes rather than participants or protocol variability. However, SRTM modelling method and FLWM as an alternative reference region are not to be totally discarded. Indeed, the choice of the modelling method and of the reference region will be driven by the pathology in study. As an example, cerebellar atrophy could be a cofounding factor when using CERWM as a reference region and FLWM would be an excellent alternative. In the present study, the LREF method with CERWM as reference region were used to evaluate [^{18}F]F13640 binding patterns, as discussed below.

[^{18}F]F13640 brain binding patterns

[^{18}F]F13640 showed elevated BP values in regions known to express a high densities of 5-HT_{1A} receptors, including the raphe (median and dorsal) and cortical regions (cingulate, frontal and temporal superior) [33]. It is noteworthy that the hippocampus only showed intermediate uptake of [^{18}F]F13640 with moderate BP values. Median and dorsal raphe nuclei were regions with highest BP values but also with the most substantial variability. This could be explained by the use of manual delineation for these small brain regions on PET images [34] while other regions were amenable to automatic segmentation from the anatomical MRI images using a multi-atlas approach [26].

Interestingly, in the parametric BP images, brainstem showed some voxels with high values whereas brainstem ROI analysis showed only moderate BP as seen before. This suggests a heterogeneity of 5-HT_{1A} receptor distribution within a same region. Previous studies of F13640 (i.e., befiradol or NLX-112) already

showed pharmacological actions in “parts” of the brainstem confirming this potential heterogeneity [35]. Thus, voxel-based analysis should be done when considering analysis between healthy volunteers and patients to detect differences in more focal sub-regions.

[^{18}F]F13640 binding in cerebellum grey matter

As described above and in an unexpected manner, cerebellum grey matter and vermis both showed high BP values. Whereas a high expression of 5-HT$_{1A}$ receptors has been described in vermis [36, 37], it is frequently postulated that cerebellum grey matter does not express 5-HT$_{1A}$ receptors. Indeed, according to post-mortem autoradiographic studies [38, 39], 5-HT$_{1A}$ receptors are expressed in fetal and neonatal stages but not in adults [40]. The present unexpected binding of [^{18}F]F13640 in cerebellum could thus question its target specificity, but interaction with a possible off-target seems unlikely based on well-documented in vitro studies [20]. Moreover, our previous preclinical studies also showed [^{18}F]F13640 binding in cerebellum in different species [21, 22] and, in all these studies, co-administration of pharmacologically relevant doses of a 5-HT$_{1A}$ receptor agonist (8-OH-DPAT) or of an antagonist (WAY-100635) inhibited [^{18}F]F13640 binding, indicating that its binding in cerebellum grey matter does indeed reflect 5-HT$_{1A}$ receptor expression in this region. In addition to the present data with [^{18}F]F13640, the assumption of a total lack of 5-HT$_{1A}$ receptors in the cerebellum was already challenged by previous PET studies revealing [*carbonyl*-^{11}C]WAY-100635 binding in human cerebellum [36], with more pronounced labeling in grey matter [37]. In other studies, participants were excluded due cerebellar TACs outside the range of the control population when cerebellum was used as a reference region [41–43]. Other 5-HT$_{1A}$ receptor radiopharmaceuticals also showed marked binding in cerebellum, notably [^{11}C]CUMI-101 which showed a significant reduction of labeling following 8-OH-DPAT or WAY-100635 pre-injection [44]. Thus, 5-HT$_{1A}$ receptors are present in cerebellum grey matter, excluding the cerebellum as a reference region for [^{18}F]F13640.

[^{18}F]F13640 binding in other brain regions

In comparison with other 5-HT$_{1A}$ radiopharmaceuticals, [^{18}F]F13640 showed particularly high uptake in raphe nuclei, cortical regions and vermis in limbic and paralimbic regions. Although [^{18}F]MPPF also showed high uptake in raphe nuclei, it preferentially binds to limbic areas such as hippocampus and amygdala whereas cortical regions showed less uptake [34]. Another antagonist radiopharmaceutical, [*carbonyl*-^{11}C]WAY-100635, also showed high binding in raphe and frontal cortex (like [^{18}F]F13640) but it also showed marked binding to hippocampus (like[^{18}F]MPPF) [3]. Binding differences between [*carbonyl*-^{11}C]WAY-100635, [^{18}F]MPPF and [^{18}F]F13640 could be explained by the pharmacological difference between these 5-HT$_{1A}$ receptor radiopharmaceuticals [45, 46]. We hypothesize that some regions such as hippocampus, which showed high uptake with antagonist radiopharmaceuticals and less with the agonist [^{18}F]F13640, express a high proportion of G-protein uncoupled 5-HT$_{1A}$ receptors. In contrast, regions with higher [^{18}F]F13640 binding values, like cingulate cortex, frontal cortex or vermis, may express a relatively higher proportion of functionally active, G-protein-coupled receptors. Finally, regions such as raphe which showed high binding with both antagonist and agonist radiopharmaceuticals may express both states of 5-HT$_{1A}$ receptors. Thus, differences in receptor binding pattern can be found between agonists and antagonists radiopharmaceuticals targeting

the same receptor. An in vitro study using [^{18}F]F13640 and [^{18}F]MPPF already explored this hypothesis and showed differences in binding between agonists and antagonists radiotracer with 5-HT$_{1A}$ in Alzheimer's disease [47]. Similar results were found with $D_{2/3}$ dopamine receptors, for which the agonist, [^{3}H]NPA, showed a greater extent of WHAT than the antagonist [^{11}C]raclopride binding in a rat Parkinson's disease model [48].

Perspectives opened by [^{18}F]F13640

[^{18}F]F13640 has now the status of a radiopharmaceutical whose pharmacokinetic and radiopharmacological characteristics offer new perspectives in neurology and psychiatry.

First of all, the sustained binding of [^{18}F]F13640 will allow studies to be performed with multiple scans at different acquisition time points on the same day. This experimental paradigm could, for example, allow exploration of changes in receptor coupling states associated with circadian rhythms. As an illustration, a previous preclinical study demonstrated that [^{18}F]F13640 is sensitive to fluctuations in serotonin levels [22] opening the way for exploration of *in vivo* serotonin release in physiological or pathological processes.

As demonstrated in this study, [^{18}F]F13640 binding using LREF method showed excellent test-retest parameters. Since reproducibility and reliability of the PET measurements is crucial for studies involving repeated measurements on the same subject, such as drug occupancy studies, intervention studies or exploring pathological states at different time points, [^{18}F]F13640 will be perfectly adapted to these approaches.

In terms of radiopharmacological characteristics, the binding pattern of [^{18}F]F13640 opens up several applications in neurology and psychiatry. As preliminary examples, [^{18}F]F13640 shows high binding values in raphe, consistent with the therapeutic-like activity of NLX-112 in rodent and non-human primate models of L-DOPA-induced dyskinesia (LID) in Parkinson's disease [49–51] which is the focus of an ongoing clinical study (ClinicalTrials.gov Identifier: NCT05148884). Indeed, targeting of raphe-localized 5-HT$_{1A}$ autoreceptors is the mechanism considered to reduce the 'false neurotransmitter' release of dopamine from 5-HT neurons that underlies LID.

[^{18}F]F13640 also shows high binding values in cortical regions associated with control of mood and cognition. Indeed, local administration of a 5-HT$_{1A}$ receptor agonist in rat cortex elicited robust antidepressant-like activity [52] and activation of cortical 5-HT$_{1A}$ receptors is associated with beneficial activity on negative symptoms of schizophrenia [53, 54]. 5-HT$_{1A}$ receptors in the brainstem are promising targets to alleviate respiratory dysfunction in disorders such as Rett syndrome [55]. [^{18}F]F13640 could therefore be an interesting tool to assess the pharmacological profile of future biased agonists candidates [15].

Conclusion

The present study reports the first-in-human validation and full kinetic modelling of [^{18}F]F13640 as the first 5-HT$_{1A}$ receptor agonist usable as a PET radiopharmaceutical. [^{18}F]F13640 shows many favorable

radiopharmacological and radiopharmaceutical characteristics: radiolabeling with fluorine-18, high selectivity over cross-reacting sites, high reproducibility and long-term binding which facilitates the experimental protocols. [^{18}F]F13640 shows pronounced binding in raphe nuclei and cortical regions, with notable differences in comparison with the classical antagonist PET radiopharmaceuticals. All these characteristics confirm the interest of developing an agonist radiotracer able to target specifically functionally active 5-HT$_{1A}$ receptors in studies with long-term scans, test-retest protocols or diseases in neurology and psychiatry.

Declarations

ACKNOWLEDGMENT

This work was supported by the LABEX PRIMES of Université de Lyon. PC was awarded a scholarship for the French Fund for Medical Research FRM (FDM202006011252).

COMPLIANCE WITH ETHICAL STANDARDS

Funding: This study was funded by by AVIESAN-ITMO Technologies for health, by the Hospices Civils de Lyon, by the imaging platform CERMEP.

Conflict of Interest: AN-T is shareholder and employee of Neurolixis. The other authors have no disclosures or conflict of interest.

Ethical approval: All procedures performed in studies involving human participants were in accordance with the ethical standards of the institutional and/or national research committee and with the 1964 Helsinki declaration and its later amendments or comparable ethical standards.

Informed consent: Informed consent was obtained from all individual participants included in the study.

References

1. Polter AM, Li X. 5-HT1A receptor-regulated signal transduction pathways in brain. Cell Signal. 2010;22:1406–12.
2. Pike VW, McCarron JA, Lammerstma AA, Hume SP, Poole K, Grasby PM, et al. First delineation of 5-HT1A receptors in human brain with PET and [11C]WAY-100635. Eur J Pharmacol. 1995;283:R1–3.
3. Gunn RN, Sargent PA, Bench CJ, Rabiner EA, Osman S, Pike VW, et al. Tracer Kinetic Modeling of the 5-HT1AReceptor Ligand [carbonyl-11C]WAY-100635 for PET. NeuroImage. 1998;8:426–40.
4. Zhuang Z-P, Kung M-P, Kung HF. Synthesis And Evaluation of 4-(2'-Methoxyphenyl)-1-[2'-[N-(2"-pyridinyl)-p-iodobenzamido]ethyl]piperazine (p-MPPI): A New Iodinated 5-HT1A Ligand. J Med Chem. 1994;37:1406–7.
5. Passchier J, van Waarde A, Pieterman RM, Elsinga PH, Pruim J, Hendrikse HN, et al. Quantitative imaging of 5-HT(1A) receptor binding in healthy volunteers with [(18)f]p-MPPF. Nucl Med Biol. 2000;27:473–6.
6. Passchier J, van Waarde A, Pieterman RM, Elsinga PH, Pruim J, Hendrikse HN, et al. In vivo delineation of 5-HT1A receptors in human brain with [18F]MPPF. J Nucl Med. 2000;41:1830–5.

7. Costes N, Merlet I, Ostrowsky K, Faillenot I, Lavenne F, Zimmer L, et al. A ^{18}F-MPPF PET Normative Database of 5-HT$_{1A}$ Receptor Binding in Men and Women Over Aging. J Nucl Med. 2005;46:1980.
8. Merlet I, Ostrowsky K, Costes N, Ryvlin P, Isnard J, Faillenot I, et al. 5-HT1A receptor binding and intracerebral activity in temporal lobe epilepsy: an [18F]MPPF-PET study. Brain. 2004;127:900–13.
9. Derry C, Benjamin C, Bladin P, le Bars D, Tochon-Danguy H, Berkovic SF, et al. Increased serotonin receptor availability in human sleep: evidence from an [18F]MPPF PET study in narcolepsy. NeuroImage. 2006;30:341–8.
10. Kepe V, Barrio JR, Huang S-C, Ercoli L, Siddarth P, Shoghi-Jadid K, et al. Serotonin 1A receptors in the living brain of Alzheimer's disease patients. Proc Natl Acad Sci U S A. 2006;103:702–7.
11. Meyer M, Lamare F, Asselineau J, Foubert-Samier A, Mazère J, Zanotti-Fregonara P, et al. Brain 5-HT1A Receptor Binding in Multiple System Atrophy: An [18 F]-MPPF PET Study. Mov Disord. 2021;36:246–51.
12. Billard T, Bars D, Zimmer L. PET Radiotracers for Molecular Imaging of Serotonin 5-HT$_{1A}$ Receptors. CMC. 2013;21:70–81.
13. Gozlan H, Thibault S, Laporte AM, Lima L, Hamon M. The selective 5-HT1A antagonist radioligand [3H]WAY 100635 labels both G-protein-coupled and free 5-HT1A receptors in rat brain membranes. Eur J Pharmacol. 1995;288:173–86.
14. Watson J, Collin L, Ho M, Riley G, Scott C, Selkirk JV, et al. 5-HT(1A) receptor agonist-antagonist binding affinity difference as a measure of intrinsic activity in recombinant and native tissue systems. Br J Pharmacol. 2000;130:1108–14.
15. Newman-Tancredi A, Depoortère RY, Kleven MS, Kołaczkowski M, Zimmer L. Translating biased agonists from molecules to medications: Serotonin 5-HT1A receptor functional selectivity for CNS disorders. Pharmacology & Therapeutics. 2021;107937.
16. Hendry N, Christie I, Rabiner EA, Laruelle M, Watson J. In vitro assessment of the agonist properties of the novel 5-HT1A receptor ligand, CUMI-101 (MMP), in rat brain tissue. Nucl Med Biol. 2011;38:273–7.
17. Shrestha SS, Liow J-S, Lu S, Jenko K, Gladding RL, Svenningsson P, et al. ^{11} C-CUMI-101, a PET Radioligand, Behaves as a Serotonin 1A Receptor Antagonist and Also Binds to α $_1$ Adrenoceptors in Brain. J Nucl Med. 2014;55:141–6.
18. Selvaraj S, Turkheimer F, Rosso L, Faulkner P, Mouchlianitis E, Roiser JP, et al. Measuring endogenous changes in serotonergic neurotransmission in humans: a [11C]CUMI-101 PET challenge study. Mol Psychiatry. 2012;17:1254–60.
19. Girgis RR, Forbes A, Abi-Dargham A, Slifstein M. A positron emission tomography occupancy study of brexpiprazole at dopamine D2 and D3 and serotonin 5-HT1A and 5-HT2A receptors, and serotonin reuptake transporters in subjects with schizophrenia. Neuropsychopharmacology. 2020;45:786–92.
20. Colpaert FC, Tarayre JP, Koek W, Pauwels PJ, Bardin L, Xu X-J, et al. Large-amplitude 5-HT1A receptor activation: a new mechanism of profound, central analgesia. Neuropharmacology. 2002;43:945–58.
21. Vidal B, Fieux S, Colom M, Billard T, Bouillot C, Barret O, et al. 18F-F13640 preclinical evaluation in rodent, cat and primate as a 5-HT1A receptor agonist for PET neuroimaging. Brain Struct Funct. 2018;223:2973–88.

22. Colom M, Vidal B, Fieux S, Redoute J, Costes N, Lavenne F, et al. [18F]F13640, a 5-HT1A Receptor Radiopharmaceutical Sensitive to Brain Serotonin Fluctuations. Front Neurosci. 2021;15:622423.
23. Mérida I, Reilhac A, Redouté J, Heckemann RA, Costes N, Hammers A. Multi-atlas attenuation correction supports full quantification of static and dynamic brain PET data in PET-MR. Phys Med Biol. 2017;62:2834–58.
24. Reilhac A, Merida I, Irace Z, Stephenson MC, Weekes AA, Chen C, et al. Development of a Dedicated Rebinner with Rigid Motion Correction for the mMR PET/MR Scanner, and Validation in a Large Cohort of ^{11} C-PIB Scans. J Nucl Med. 2018;59:1761–7.
25. Heckemann RA, Keihaninejad S, Aljabar P, Rueckert D, Hajnal JV, Hammers A. Improving intersubject image registration using tissue-class information benefits robustness and accuracy of multi-atlas based anatomical segmentation. NeuroImage. 2010;51:221–7.
26. Hammers A, Allom R, Koepp MJ, Free SL, Myers R, Lemieux L, et al. Three-dimensional maximum probability atlas of the human brain, with particular reference to the temporal lobe. Hum Brain Mapp. 2003;19:224–47.
27. Gousias IS, Rueckert D, Heckemann RA, Dyet LE, Boardman JP, Edwards AD, et al. Automatic segmentation of brain MRIs of 2-year-olds into 83 regions of interest. NeuroImage. 2008;40:672–84.
28. Faillenot I, Heckemann RA, Frot M, Hammers A. Macroanatomy and 3D probabilistic atlas of the human insula. NeuroImage. 2017;150:88–98.
29. Logan J. Graphical analysis of PET data applied to reversible and irreversible tracers. Nucl Med Biol. 2000;27:661–70.
30. Gunn RN, Lammertsma AA, Hume SP, Cunningham VJ. Parametric Imaging of Ligand-Receptor Binding in PET Using a Simplified Reference Region Model. NeuroImage. 1997;6:279–87.
31. Shrout PE, Fleiss JL. Intraclass correlations: uses in assessing rater reliability. Psychol Bull. 1979;86:420–8.
32. Kegeles LS, Slifstein M, Xu X, Urban N, Thompson JL, Moadel T, et al. Striatal and Extrastriatal Dopamine D2/D3 Receptors in Schizophrenia Evaluated With [18F]fallypride Positron Emission Tomography. Biol Psychiatry. 2010;68:634–41.
33. Barnes NM, Sharp T. A review of central 5-HT receptors and their function. Neuropharmacology. 1999;38:1083–152.
34. Costes N, Merlet I, Zimmer L, Lavenne F, Cinotti L, Delforge J, et al. Modeling [18 F]MPPF positron emission tomography kinetics for the determination of 5-hydroxytryptamine(1A) receptor concentration with multiinjection. J Cereb Blood Flow Metab. 2002;22:753–65.
35. Vidal B, Fieux S, Redouté J, Villien M, Bonnefoi F, Le Bars D, et al. In vivo biased agonism at 5-HT1A receptors: characterisation by simultaneous PET/MR imaging. Neuropsychopharmacol. 2018;43:2310–9.
36. Parsey RV, Arango V, Olvet DM, Oquendo MA, Van Heertum RL, Mann JJ. Regional Heterogeneity of 5-HT $_{1A}$ Receptors in Human Cerebellum as Assessed by Positron Emission Tomography. J Cereb Blood Flow Metab. 2005;25:785–93.
37. Hirvonen J, Kajander J, Allonen T, Oikonen V, Någren K, Hietala J. Measurement of Serotonin 5-HT1A Receptor Binding Using Positron Emission Tomography and [*carbonyl* – ^{11} C]WAY-100635—

Considerations on the Validity of Cerebellum as a Reference Region. J Cereb Blood Flow Metab. 2007;27:185–95.

38. Hall H, Lundkvist C, Halldin C, Farde L, Pike VW, McCarron JA, et al. Autoradiographic localization of 5-HT1A receptors in the post-mortem human brain using [3H]WAY-100635 and [11C]way-100635. Brain Res. 1997;745:96–108.
39. Pazos A, Probst A, Palacios JM. Serotonin receptors in the human brain—III. Autoradiographic mapping of serotonin-1 receptors. Neuroscience. 1987;21:97–122.
40. del Olmo E, Díaz A, Guirao-Piñeyro M, del Arco C, Pascual J, Pazos A. Transient localization of 5-HT1A receptors in human cerebellum during development. Neurosci Lett. 1994;166:149–52.
41. Doder M, Rabiner EA, Turjanski N, Lees AJ, Brooks DJ. Tremor in Parkinson's disease and serotonergic dysfunction: An ^{11} C-WAY 100635 PET study. Neurology. 2003;60:601–5.
42. Turner MR, Rabiner EA, Hammers A, Al-Chalabi A, Grasby PM, Shaw CE, et al. [11C]-WAY100635 PET demonstrates marked 5-HT1A receptor changes in sporadic ALS. Brain. 2005;128:896–905.
43. Rabiner EA, Messa C, Sargent PA, Husted-Kjaer K, Montgomery A, Lawrence AD, et al. A Database of [11C]WAY-100635 Binding to 5-HT1A Receptors in Normal Male Volunteers: Normative Data and Relationship to Methodological, Demographic, Physiological, and Behavioral Variables. NeuroImage. 2002;15:620–32.
44. Milak MS, Severance AJ, Ogden RT, Prabhakaran J, Kumar JSD, Majo VJ, et al. Modeling Considerations for ^{11} C-CUMI-101, an Agonist Radiotracer for Imaging Serotonin 1A Receptor In Vivo with PET. J Nucl Med. 2008;49:587–96.
45. Kenakin T. Functional Selectivity through Protean and Biased Agonism: Who Steers the Ship? Mol Pharmacol. 2007;72:1393–401.
46. Perez DM, Karnik SS. Multiple Signaling States of G-Protein-Coupled Receptors. Pharmacol Rev. 2005;57:147–61.
47. Vidal B, Sebti J, Verdurand M, Fieux S, Billard T, Streichenberger N, et al. Agonist and antagonist bind differently to 5-HT 1A receptors during Alzheimer's disease: A post-mortem study with PET radiopharmaceuticals. Neuropharmacology. 2016;109:88–95.
48. Palner M, Kjaerby C, Knudsen GM, Cumming P. Effects of unilateral 6-OHDA lesions on [3H]-N-propylnorapomorphine binding in striatum ex vivo and vulnerability to amphetamine-evoked dopamine release in rat. Neurochem Int. 2011;58:243–7.
49. Iderberg H, McCreary AC, Varney MA, Kleven MS, Koek W, Bardin L, et al. NLX-112, a novel 5-HT 1A receptor agonist for the treatment of l -DOPA-induced dyskinesia: Behavioral and neurochemical profile in rat. Exp Neurol. 2015;271:335–50.
50. Depoortere R, Johnston TH, Fox SH, Brotchie JM, Newman-Tancredi A. The selective 5-HT1A receptor agonist, NLX-112, exerts anti-dyskinetic effects in MPTP-treated macaques. Parkinsonism Relat Disord. 2020;78:151–7.
51. Fisher R, Hikima A, Morris R, Jackson MJ, Rose S, Varney MA, et al. The selective 5-HT1A receptor agonist, NLX-112, exerts anti-dyskinetic and anti-parkinsonian-like effects in MPTP-treated marmosets. Neuropharmacology. 2020;167:107997.

52. Newman-Tancredi A, Bardin L, Auclair A, Colpaert F, Depoortère R, Varney MA. NLX-112, a highly selective 5-HT 1A receptor agonist, mediates analgesia and antidepressant-like activity in rats via spinal cord and prefrontal cortex 5-HT 1A receptors, respectively. Brain Res. 2018;1688:1–7.
53. Buckley PF. Neuroimaging of schizophrenia: structural abnormalities and pathophysiological implications. Neuropsychiatr Dis Treat. 2005;1:193–204.
54. Razakarivony O, Newman-Tancredi A, Zimmer L. Towards in vivo imaging of functionally active 5-HT1A receptors in schizophrenia: concepts and challenges. Transl Psychiatry. 2021;11:22.
55. Abdala AP, Bissonnette JM, Newman-Tancredi A. Pinpointing brainstem mechanisms responsible for autonomic dysfunction in Rett syndrome: therapeutic perspectives for 5-HT1A agonists. Front Physiol [Internet]. 2014 [cited 2021 Nov 24];5. Available from: http://journal.frontiersin.org/article/10.3389/fphys.2014.00205/abstract.

Figures

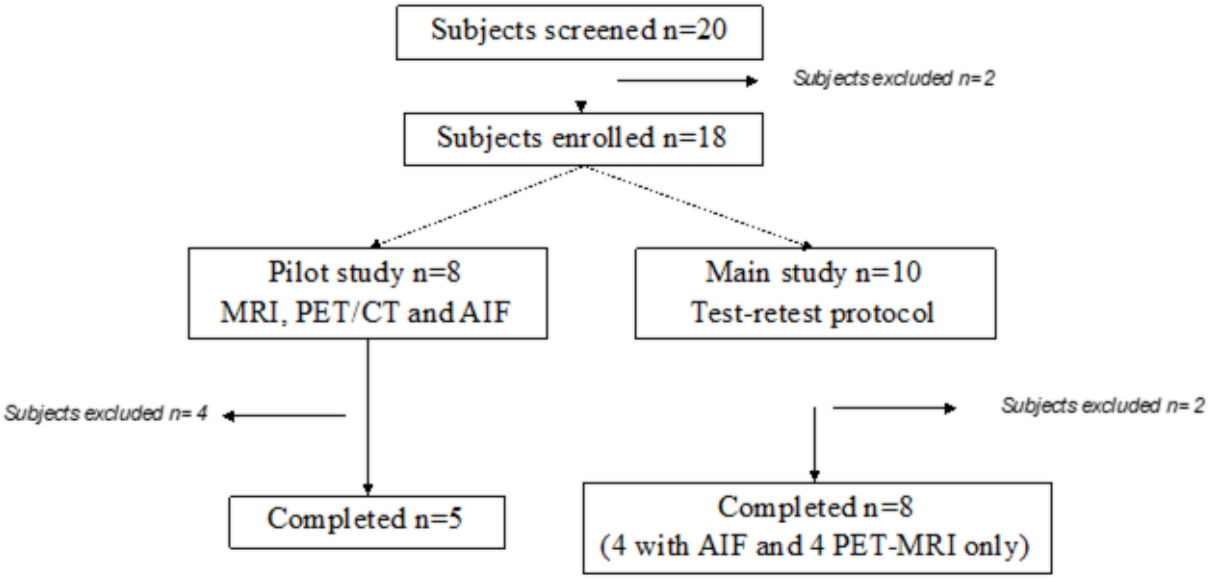

Figure 1

Summary flow-chart of healthy subjects' inclusion for pilot study and main test-retest study. Analysis focused only on the 8 PET-MRI subjects and 4 PET-MRI subjects when AIF is considering.

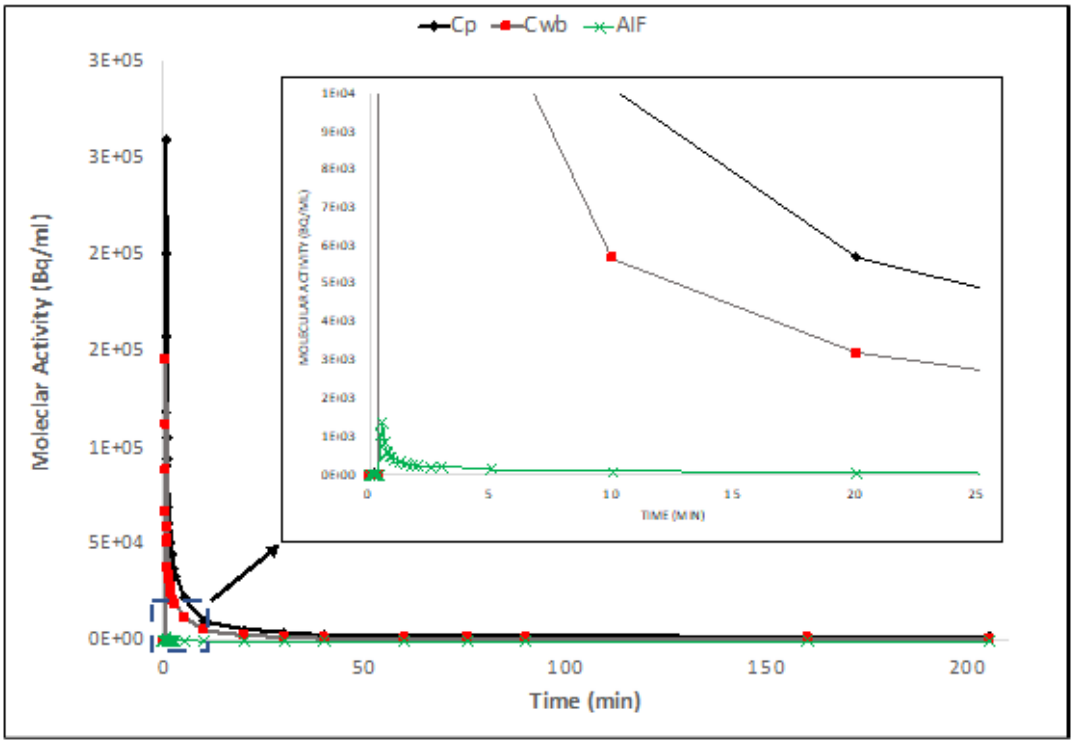

Figure 2

Example of an arterial input function (AIF) for a subject with whole blood (Cwb) and uncorrected plasma curve (Cp).

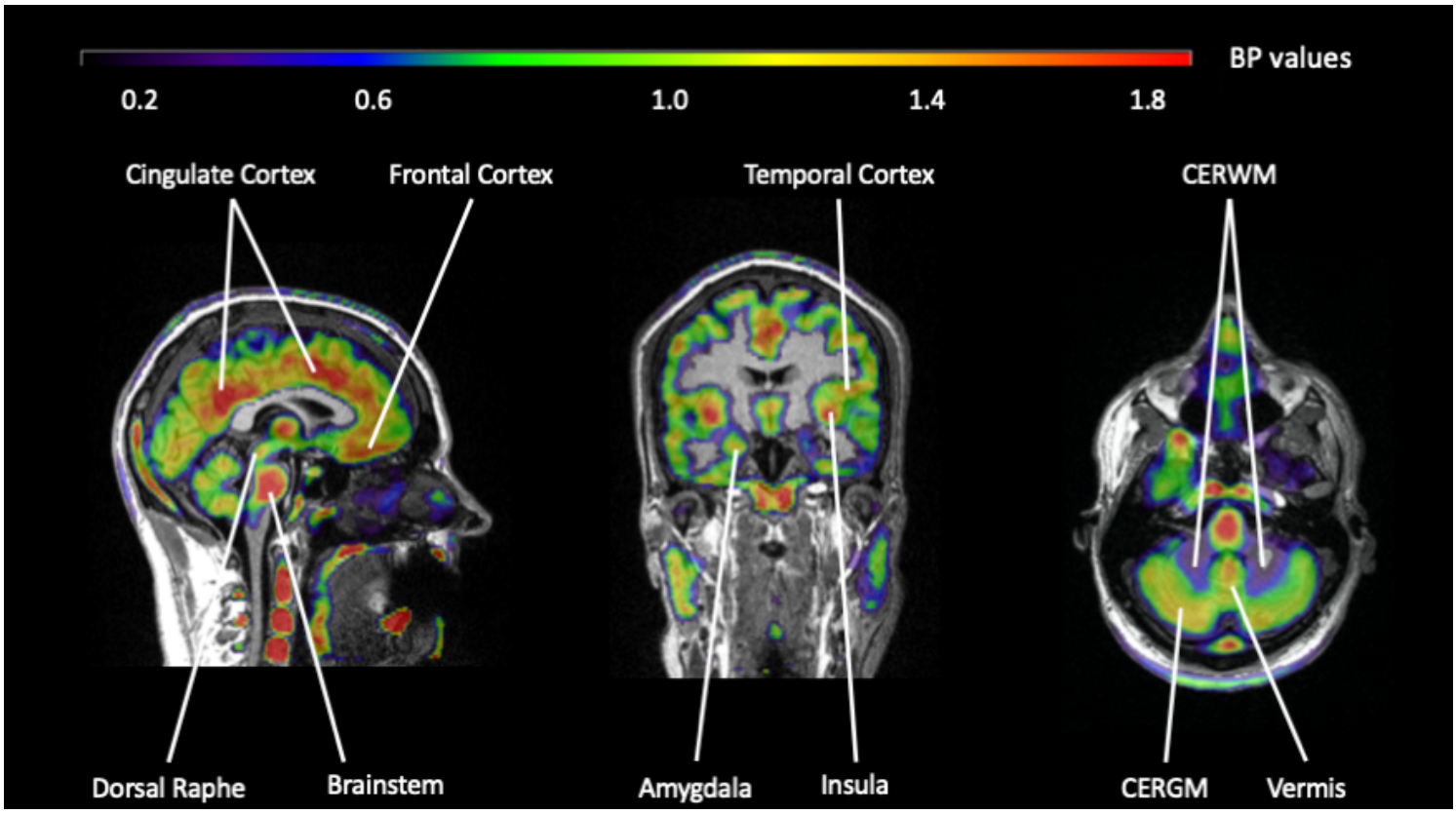

Figure 3

Parametric image of BP values estimated with $LREF_{CERWM}$. BP image is overlaid on the T1 MRI of the participant (CERWM = cerebellum white matter; CERGM = cerebellum grey matter).

Supplementary Files

This is a list of supplementary files associated with this preprint. Click to download.

- Onlineresource1.docx